Polymer Interphase Materials by Forced Assembly

R. Y. F. Liu,† T. E. Bernal-Lara,‡ A. Hiltner,* and E. Baer

Department of Macromolecular Science, and Center for Applied Polymer Research, Case Western Reserve University, Cleveland, Ohio 44106-7202

Received December 31, 2004; Revised Manuscript Received March 25, 2005

ABSTRACT: The interphase between two immiscible glassy polymers was probed using nanolayer films with tens to thousands of alternating layers of two polymers. Various combinations of poly(methyl methacrylate), polycarbonate, and a series of styrene−acrylonitrile copolymers were brought together by forced assembly. Continuous nanolayers with thickness on the size scale of the interphase were observed directly using atomic force microscopy. Interphase thickness was extracted from the layer thickness dependence of oxygen permeability. The interphase thickness showed the predicted dependence on the χ interaction parameter and correlated with interphase strength as measured with the T-peel test. Interphase specific volume, as determined by density, exhibited both positive and negative deviations from constituent additivity. The deviations correlated with the change in free volume hole size from positron annihilation lifetime spectroscopy but did not correlate directly with the χ parameter. The origin of the deviations was found in the nature of chain packing in the interphase, as evidenced by nonadditivity in entanglement molecular weight. The volumetric effects accounted for the glass transition behavior of the interphase material.

Introduction

When two immiscible polymers are brought into intimate contact, highly localized mixing of polymer chains creates an "interphase" region. The driving force for interfacial mixing is the entropic advantage for chains to diffuse across the interfacial boundary. The entropic advantage for crossing the interface is offset by the repulsive interaction energy between immiscible chain segments. A vast literature attests to the importance of the interphase for polymer adhesion and for compatibility of polymer blends and alloys.[1]

Until recently, experimental determination of interphase properties was a challenge due to the extremely small volume fraction of interphase in a typical polymer blend. Even measurement of the interphase dimension was difficult and required extreme care. Nevertheless, existing theoretical and experimental results agreed that the dimension of the interphase for immiscible polymers could range from a few to tens of nanometers.[1−3] Other physical properties of the interphase, such as density, free volume, and permeability, remained virtually inaccessible experimentally.

In previous publications, we describe the use of forced assembly to fabricate materials that are entirely interphase. Films comprised of thousands of alternating layers of two polymers, with individual layer thickness on the nanometer size scale of the interphase, are created by layer multiplying coextrusion.[4,5] An initial study describes the effects of layer thickness on assemblies of two immiscible glassy polymers, polycarbonate (PC) and poly(methyl methacrylate) (PMMA).[6] In conventional DSC thermograms the two glass transition inflections of the constituent polymers shift closer together as layer thickness decreases below 100 nm and merge into a single inflection when the layer thickness is 10 nm or less. This result demonstrates that as layer thickness becomes comparable to the interphase dimension, individual layers lose their integrity as constituent layers and the film essentially becomes totally interphase. A new type of interphase material is created.

The effect of interaction strength is probed further in a subsequent study of assemblies that combine an amorphous polyester with a series of styrene−acrylonitrile copolymers.[7] The interphase thickness, extracted from the layer thickness dependence of oxygen permeability, shows the predicted dependency on the χ parameter and correlates with interphase strength. However, volumetric properties of density and free volume hole size show unexpected deviations from additivity based on constituent properties. Moreover, the deviations do not correlate with the χ parameter.

This paper extends the established methodology to probe the interphase of other immiscible polymer pairs based on poly(methyl methacrylate) (PMMA), polycarbonate (PC), and a series of styrene−acrylonitrile copolymers (SAN) that vary in acrylonitrile content. We use the layer thickness dependence of oxygen permeability to determine the interphase dimension of the various polymer pairs and compare the results with theoretical predictions. Density, free volume hole size, glass transition temperature, and entanglement molecular weight of interphase materials and discrete layer films are compared in order to address the physical origin of volumetric changes upon segmental mixing.

Materials and Methods

Polycarbonate (PC) was provided by The Dow Chemical Company (Calibre 200-10). Poly(methyl methacrylate) (PMMA) was provided by Atofina Chemicals, Inc. (Plexiglas V826). An amorphous polyester, poly(ethylene terephthalate-*co*-1,4-cyclohexanedimethylene terephthalate) (PETG), was provided by Eastman Chemical Co. (Eastar 6763). Polystyrene (PS) was supplied by The Dow Chemical Company (Styron 685D). Styrene−acrylonitrile copolymers (SAN25 and SAN30) were supplied by The Dow Chemical Company (Tyril 100 and Tyril 880, respectively). The number following the SAN abbreviation represents the weight percent acrylonitrile in the copolymer as given by the manufacturer and confirmed by infrared spectroscopy.[8] The resins were received in the form of pellets and used without further purification. The molecular weight

† Present address: 3M, St. Paul, MN 55144.
‡ Present address: The Dow Chemical Company, Freeport, TX 77541.
* Corresponding author: e-mail pah6@case.edu.

10.1021/ma047292z CCC: $30.25
Published on Web 04/30/2005

Table 1. Physical Properties of Constituent Glassy Polymers[a]

polymer	δ	ρ	T_g (DSC)	T_g (DMTA)	P	r	M_w	PDI	M_e	M_e (lit.)
PC	19.59	1.1934	145	157	9.91	2.82	62	1.6	1.2	1.3[c]
PMMA	19.89	1.1923	112	120	0.371	2.71	132	1.3	6.6	10[c]
PETG	19.70	1.2796	82	87	0.750	2.52	87		1.3	
PS	18.41[b]	1.0450	102	108	14.5	2.85	527	1.7	13	13[c]
SAN17	19.36[b]	1.0700	103	110	5.54	2.76	159	1.4	7.4	
SAN25	20.01[b]	1.0800	107	114	3.36	2.73	269	1.9	6.7	
SAN30	20.26[b]	1.0856	108	116	2.63	2.72	286	1.8	6.0	

[a] δ = solubility parameter in $J^{0.5}$ cm$^{-1.5}$. ρ = density in g cm^{-3}. T_g = glass transition temperature in °C. P = permeability in cm^3 (STP) cm m^{-2} day^{-1} atm^{-1}. r = free volume hole radius in Å. M_w = molecular weight in kg mol^{-1}. PDI = polydispersity index. M_e = entanglement molecular weight in kg mol^{-1}. ρ, T_g(DSC), T_g(DMTA), P, r, and M_e measured on 32-layer control films. [b] From ref 16. [c] From ref 38.

Table 2. Properties of Discrete Layers and Interphase Material[a]

constituent polymers	T_p (°C)	χ (10^{-3})	d_I (nm)	P_d	P_h	P_I	ρ_d (g cm^{-3})	ρ_I (g cm^{-3})	r_d (Å)	r_I (Å)	G_{IC} (J m^{-2})
PMMA/PS	260	45	6.1	0.710	2.32		1.1187	1.1161[b]	2.80	2.85[b]	45 ± 11
PMMA/SAN25	260	0.28	33	0.679	1.12	1.26	1.1316	1.1299	2.72	2.74	
PMMA/SAN30	260	2.4	8.0	0.639	0.988	1.12	1.1344	1.1324	2.72	2.76	80 ± 10
PC/PMMA[c]	270	2.3	10	0.720	1.92	1.62	1.1928	1.1945	2.76	2.71	
PC/PETG	260	0.45	27	1.43	2.73	2.71	1.2365	1.2389	2.67	2.63	
PC/SAN25	260	4.5	7.5	5.01	5.77	6.30	1.1346	1.1402	2.79	2.70	83 ± 15
PETG/PS[d]	240	47	3.8	1.43	3.30		1.1624	1.1677	2.71	2.63	15 ± 5
PETG/SAN17[d]	240	2.9	8.9	1.32	2.03	1.91	1.1732	1.1790	2.64	2.55	61 ± 10
PETG/SAN25[d]	240	2.4	11	1.23	1.59	1.56	1.1796	1.1805	2.63	2.59	70 ± 10
PETG/SAN30[d]	240	7.3	6.9	1.17	1.40	1.38	1.1815	1.1902	2.63	2.50	41 ± 6

[a] χ = interaction parameter, d_I = interphase thickness, P_d = permeability of discrete layers in cm^3 (STP) cm m^{-2} day^{-1} atm^{-1}, P_h = permeability of homogeneous mixture from eq 2 in cm^3 (STP) cm m^{-2} day^{-1} atm^{-1}, P_I = permeability of interphase in cm^3 (STP) cm m^{-2} day^{-1} atm^{-1}, ρ_d = density of discrete layers, ρ_I = density of interphase, r_d = free volume hole radius of discrete layers, r_I = free volume hole radius of interphase, and G_{IC} = interphase strength. [b] Film with 84% interphase. [c] From ref 6. [d] From ref 7.

of PC, PMMA, PS, and SAN copolymers was determined using GPC. The instrument was calibrated with polystyrene standards. The M_w and polydispersity index PDI = M_w/M_n are given in Table 1.

Films were fabricated using the layer-multiplication process described previously.[9,10] Extruder temperatures were adjusted to ensure that the viscosities matched when the melts were combined in the feedblock. Metering pumps ensured that the feed ratio was 1:1 (v:v). The processing temperature T_p for each assembly is listed in Table 2. After the melt exited the assembly of n die elements with $2^{(n+1)}$ layers, it was spread in a film die to further reduce the layer thickness. Rapid quenching on a chill roll equipped with an air knife froze the melt morphology. Films composed of alternating layers of PETG and either PS or SAN were processed into 32 layers (4 die elements), 512 layers (8 die elements), and 4096 layers (11 die elements) with total film thickness ranging from 20 to 400 μm. The controls were 32-layer films prepared by coextrusion with the constituent polymer in both extruders. The nominal layer thickness d_0 was taken as the film thickness divided by the number of layers and ranged from more than 10 μm to a few nanometers. The isotropic nature of the nanolayer films was confirmed by the isotropic amorphous halo in X-ray patterns and identical refractive indices in machine, transverse, and thickness directions. The thinnest layers were less than the end-to-end distance of the polymer molecule (20−50 nm).

For atomic force microscopy (AFM), a film was embedded in 5 min epoxy and cured overnight at 23 °C. Cured specimens were sectioned perpendicular to the plane of the film with an ultramicrotome (MT6000-XL from RMC, Tucson, AZ). The surfaces were examined at ambient conditions using the tapping mode of the Nanoscope IIIa MultiMode scanning probe microscope (Digital Instruments). Phase and height images were recorded simultaneously. Phase images most clearly revealed the layered film structure. To resolve the layer structure at the nanoscale, measurements were performed using Si probes with a spring constant of 50 N m^{-1} and resonance frequency in the 284−362 kHz range. The probe radius was 5−10 nm.

The glass transition temperature T_g of the constituent polymers was determined by differential scanning calorimetry (DSC). Thermograms were obtained with a Perkin-Elmer DSC-7 using a heating rate of 10 °C min^{-1}.

The density was measured with a density gradient column constructed from an aqueous solution of calcium nitrate in accordance with ASTM-D 1505 method B. The column was calibrated with glass floats of known density. Small pieces of film (~25 mm^2) were placed in the column and allowed to equilibrate for 30 min before the measurements were taken. The standard deviation was within ±0.0005 g cm^{-3} for four specimens.

Positron annihilation lifetime spectroscopy (PALS) was performed at 23 °C using a conventional fast−fast coincidence system. The instrumentation and procedures for data analysis were described previously.[11] Ten spectra were collected for each specimen, and the standard deviation of the resulting mean free volume hole radius was within ±0.01 Å.

The oxygen flux $J(t)$ at 0% relative humidity, pressure p of 1 atm, and 23 °C was measured with a MOCON OX-TRAN 2/20. The instrument was calibrated using NIST certified Mylar films of known transport characteristics. To obtain accurate permeability, given by $P = Jl/p$, the average thickness l of each specimen was determined as $l = W(A\rho)^{-1}$, where W is the weight, A is the area, and ρ is the density. The error in determining permeability was estimated not to exceed 3%.

Interfacial strength was measured at 23 °C with the T-peel test (ASTM D 1876) using 400 μm thick films with 32 layers. The nominal layer thickness was 12.5 μm. To initiate crack propagation, specimens 10 mm wide were notched at the center. Peel tests were conducted with a 500 g load cell in a universal testing machine (Instron 1123) at a crosshead speed of 10 mm min^{-1}. For each composition, 5−7 specimens were tested. The crack propagated at a relatively constant load P_{cr} from which the delamination strength, given as $G_{IC} = 2P_{cr}/W$, was obtained for a specimen of width W. Decreasing the crosshead speed had almost no effect on G_{IC}. The beam arms returned to their original position upon removal of the load, indicating that the contribution of beam arm deformation to delamination strength was negligible. The peeled surfaces were characterized with a Nicolet 870 Nexus FT-IR spectrometer with a photoacoustic attachment (FTIR-PAS). The penetration depth of the acoustic signal was in the range 3−5 μm, which was significantly smaller than the individual layer

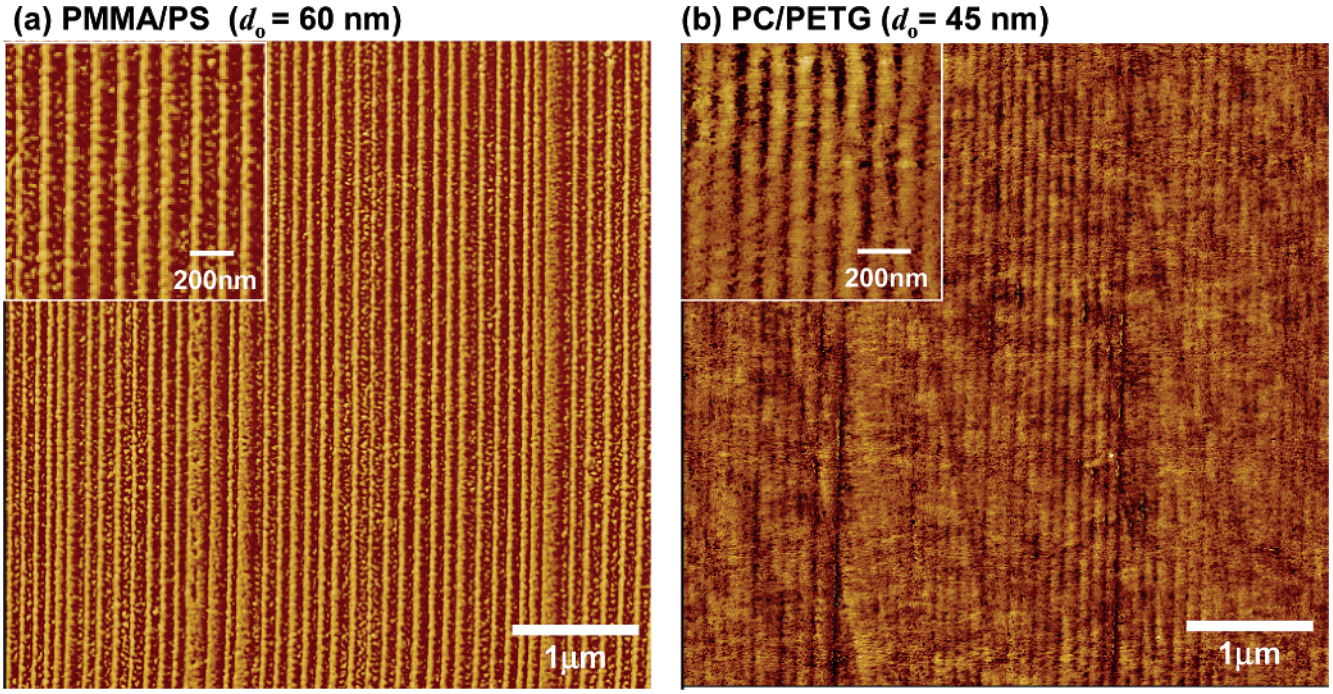

Figure 1. AFM phase images of film cross sections: (a) PMMA/PS with nominal layer thickness of 60 nm and (b) PC/PETG with nominal layer thickness of 45 nm.

thickness of 12.5 μm. The peeled surfaces were also examined by scanning electron microscopy (SEM) (JEOL 840A) with about 90 Å of gold coating.

Dynamic mechanical thermal analysis (DMTA) was carried out in an Mk II unit (Polymer Laboratories, Amherst, MA) operating in the tensile mode with a frequency of 1 Hz and heating rate of 10 °C min^{-1}. For all systems except PMMA/PS, 25 μm thick films were assembled into a stack of 8−10 pieces to enhance the signal. To calculate the entanglement molecular weight M_e for constituent materials and layered assemblies, the rubbery plateau modulus E_0 was taken at the end of the glass transition tan δ peak. The estimated uncertainty in determining log E_0 was 0.1 with E_0 in Pa.

Results and Discussion

Oxygen Permeability. The films are characterized by continuous and fairly uniform layers as determined by AFM. Figure 1a,b shows phase images of PMMA/PS and PC/PETG films with layer thicknesses of 60 and 45 nm, respectively. The bright layers are PMMA in Figure 1a and PC in Figure 1b. The layer boundaries are sharp in PMMA/PS, whereas the boundaries are somewhat diffuse in PC/PETG films, suggesting a thicker interphase. In all cases, the average layer thickness measured from AFM phase images corresponds well with the nominal layer thickness d_0 calculated from film thickness and number of layers. The layer thickness is designated as d_0 in subsequent discussions.

Oxygen permeability P of PMMA/SAN25 is plotted as a function of layer thickness d_0 in Figure 2a. For layers thicker than about 300 nm, permeability is essentially independent of layer thickness. The series model for permeability of an AB layered structure of 1:1 (v:v) composition is

$$P_d = 2\left[\frac{1}{P_A^{\circ}} + \frac{1}{P_B^{\circ}}\right]^{-1} \quad (1)$$

where P_A° and P_B° are the permeabilities of A and B, respectively. The calculated permeability from eq 1 is represented by the lower dashed line in Figure 2a. The measured P of about 0.679 cm^3 (STP) cm m^{-2} day^{-1} atm^{-1} for films with layers thicker than 300 nm corresponds to P_d. Thus, the film can be described as an array of discrete layers that exhibit the constituent properties.

As the layer thickness decreases below 300 nm, the interphase becomes a larger fraction of the total volume. Correspondingly, P increases rapidly until the layer thickness is in the range of 30 nm. Further decrease in layer thickness does not affect P. The maximum P of 1.26 cm^3 (STP) cm m^{-2} day^{-1} atm^{-1} is taken as the interphase permeability P_I and is represented by the upper dashed line in Figure 2a. This value is close but not equal to the permeability of a homogeneous 1:1 (v:v) mixture P_h given as

$$\ln P_h = \frac{1}{2}(\ln P_A^{\circ} + \ln P_B^{\circ}) \quad (2)$$

For PMMA/SAN25, the calculated P_h is 1.12 cm^3 (STP) cm m^{-2} day^{-1} atm^{-1}.

To describe the gas permeability of films with layer thickness less than 300 nm and to obtain the interphase thickness d_I, films with $d_0 \geq d_I$ are assumed to possess symmetrical interphases of constant thickness d_I. The dependence of P on layer thickness is then given by a three-layer composite model in which an interphase of thickness d_I is sandwiched between constituent layers of thickness $d_0/2$

$$P = 2\left[\frac{d_0 - d_I}{d_0}\left(\frac{1}{P_A^{\circ}} + \frac{1}{P_B^{\circ}}\right) + 2\frac{d_I}{d_0}\left(\frac{1}{P_I}\right)\right]^{-1} \quad (3)$$

Equation 3 is formulated only for films with a 1:1 (v:v) composition. The first term is the contribution of the constituent layers. The second term is the interphase contribution which dominates as d_0 approaches d_I. When the layers are sufficiently thin, $d_0 < d_I$ and the film is totally interphase with permeability P_I. Taking

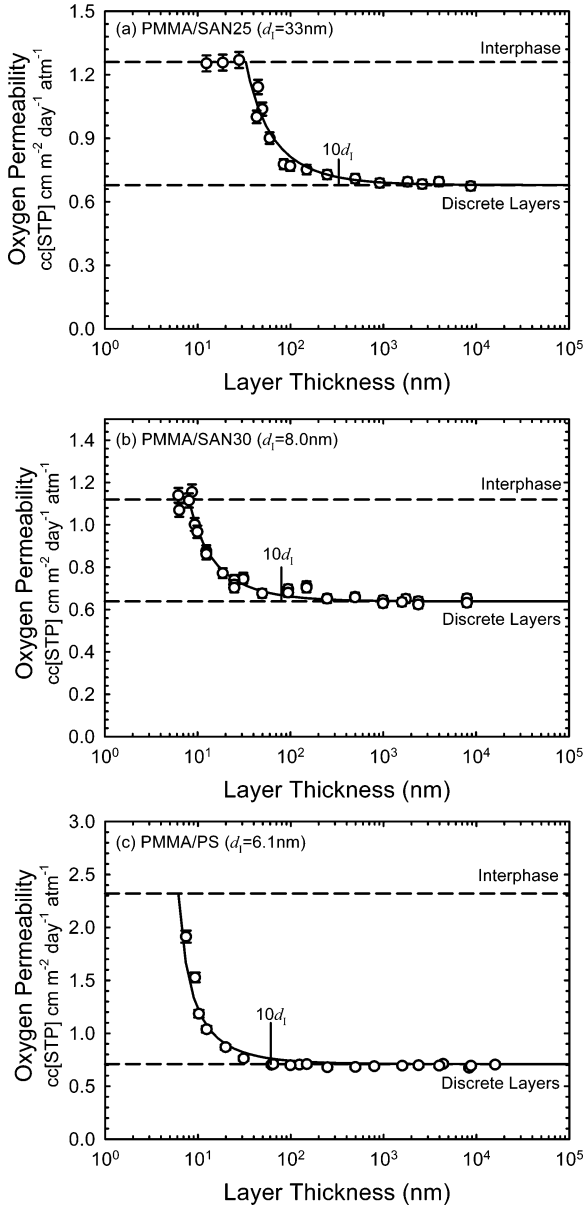

Figure 2. Effect of layer thickness on oxygen permeability: (a) PMMA/SAN25, (b) PMMA/SAN30, and (c) PMMA/PS. The solid lines indicate the best fit of the data to eq 3; the upper and lower dashed lines indicate P_I and P_d, respectively.

P_I of 1.26 cm^3 (STP) cm m^{-2} day^{-1} atm^{-1} for the PMMA/SAN25 interphase, the data for $d_0 \geq d_I$ are fit to eq 3 with the interphase thickness d_I as the only adjustable parameter. The best fit as represented by the solid line in Figure 2a is obtained with d_I of 33 nm. The fit is sensitive enough to reliably give d_I to two significant figures. Deviation from the additive value occurs when d_0 is approximately $10d_I$ (330 nm) or when the interphase is 10% of the volume.

Oxygen permeability of PMMA/SAN30 films also increases as the layer thickness approaches the nanoscale (Figure 2b); however, the deviation from the additive value of 0.639 cm^3 (STP) cm m^{-2} day^{-1} atm^{-1} begins with slightly thinner layers having d_0 of about 80 nm, indicating that PMMA/SAN30 has a slightly thinner interphase than PMMA/SAN25. The increase in P between d_0 of 80 nm and about 8 nm is described by eq 3 with d_I of 8.0 nm and P_I of 1.12 cm^3 (STP) cm m^{-2} day^{-1} atm^{-1}. The value obtained for P_I is slightly higher than P_h for the homogeneous mixture of 0.988

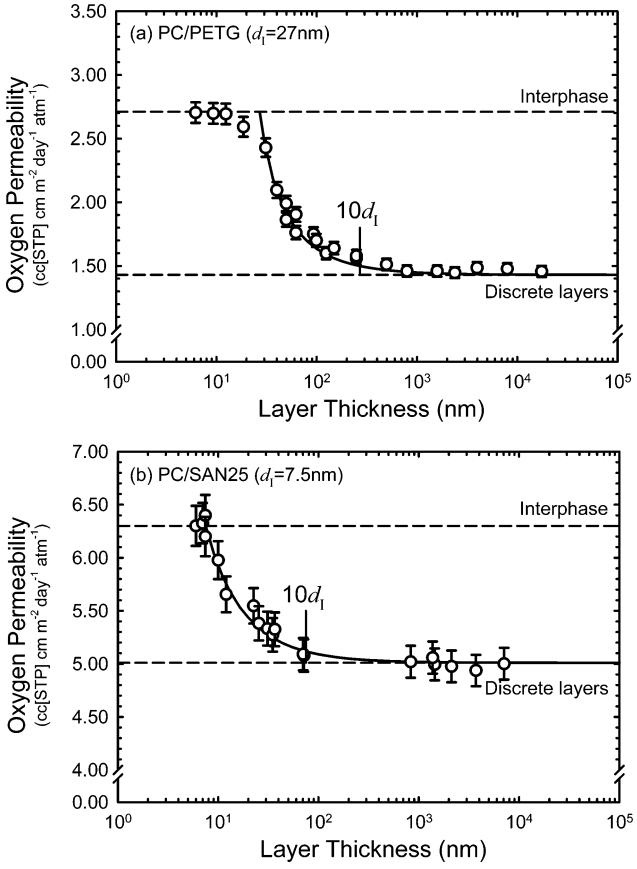

Figure 3. Effect of layer thickness on oxygen permeability: (a) PC/PETG and (b) PC/SAN25. The solid lines indicate the best fit of the data to eq 3; the upper and lower dashed lines indicate P_I and P_d, respectively.

cm^3 (STP) cm m^{-2} day^{-1} atm^{-1}. The P_h and P_I values are summarized in Table 2.

Oxygen permeability of PMMA/PS is plotted as a function of d_0 in Figure 2c. The value of 0.710 cm^3 (STP) cm m^{-2} day^{-1} atm^{-1} for films with layers thicker than about 100 nm conforms to eq 1 and is taken as P_d for this polymer pair. As d_0 decreases below about 50 nm, P increases continuously without reaching a constant value. The highest permeability measured for a PMMA/PS film is 1.97 cm^3 (STP) cm m^{-2} day^{-1} atm^{-1} for a film with the thinnest layers ($d_0 = 7.3$ nm). Despite the large increase in P compared to P_d, P of the film with 7.3 nm layers is significantly smaller than P_h from eq 2 of 2.32 cm^3 (STP) cm m^{-2} day^{-1} atm^{-1}. In this case, the interphase thickness is less than 7 nm, and a film totally comprised of interphase is not obtained. Assuming that P_h is a good approximation of P_I, eq 3 gives the interphase thickness of PMMA/PS as 6.1 nm.

The effect of layer thickness on oxygen permeability of two additional polymer pairs based on polycarbonate, PC/PETG and PC/SAN25, is shown in Figure 3. Analysis according to eq 3 gives interphase thicknesses of 27 and 7.5 nm for PC/PETG and PC/SAN25, respectively. It can be seen that the combination of PC with PETG produces a thicker interphase than the other polymer pairings.

Interphase Thickness. The self-consistent mean-field theory utilized by Helfand and co-workers quantitatively relates the segment density of polymer A across a symmetric interphase between immiscible polymers A and B of infinite molecular weight to the thermodynamic interaction parameter χ.[12–14] The analy-

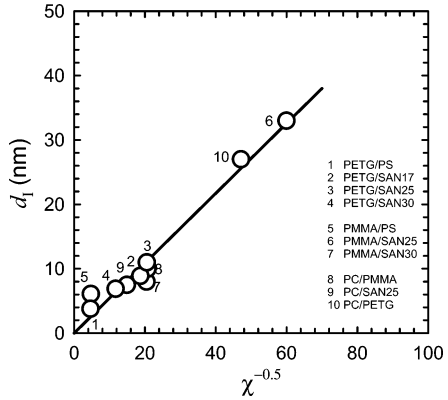

Figure 4. Relationship between interphase thickness and interaction strength as expressed by the χ parameter. The line represents the prediction given by eq 4 with $b = 5.5$ Å.

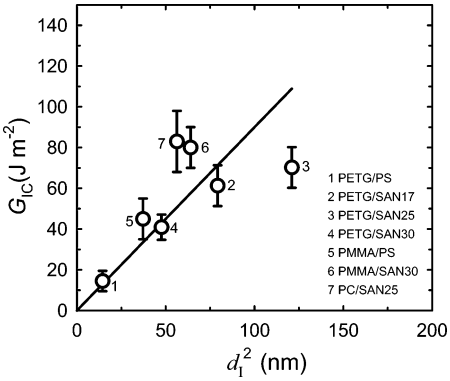

Figure 5. Relationship between interfacial strength and interphase thickness. The solid line represents the squared relationship.

sis leads to an expression for the interphase thickness d_I as

$$d_I = \frac{2b}{(6\chi)^{0.5}} \tag{4}$$

where b is the statistical segment step length and χ is the thermodynamic interaction parameter. The experimental result for d_I can be compared with the theoretical prediction if the interaction parameter χ is known. The interaction parameter χ_{AB} for the AB polymer pair is obtained from the solubility parameter of the constituents δ_A and δ_B according to the expression

$$\chi_{AB} = \frac{V}{RT}(\delta_A - \delta_B)^2 \tag{5}$$

where V is the reference molar volume taken as the average for polymers A and B, and T is taken as the processing temperature given in Table 2 for each polymer pair. Typically, χ is a small number, and therefore it is very sensitive to the choice of δ_A and δ_B. However, for any given polymer, a large range of δ values is often reported due to the relatively large method-to-method variation.[15] To minimize such effects, solubility parameters of PS and SAN copolymers are taken from the linear relationship between δ and acrylonitrile content constructed with data from a single source.[16] The δ values for PC, PMMA, and PETG are taken from previous work.[6,7] The values of δ given in Table 1 are for ambient temperature. However, assuming that the temperature dependence of δ is about the same for all the polymers studied, the quantity $(\delta_A - \delta_B)$ is essentially temperature independent. Indeed, the assumption that $(\delta_A - \delta_B)$ can be taken as a constant in eq 5 is supported by the experimental observation that χ varies as T^{-1}.[17,18]

Interphase thickness from permeability is plotted according to eq 4 in Figure 4. Results from previous studies for PC/PMMA,[6] and for PETG/PS, PETG/SAN17, PETG/SAN25, and PETG/SAN30,[4] are included. The data exhibit a good linear dependence on $\chi^{-0.5}$ with $b = 5.5$ Å. This value is close to the theoretical prediction of $b \cong 6.0$ Å.[2,13]

Interphase Strength. The strength of the interphase depends on the physical entanglement of chains crossing the interface. A minimum of one entanglement is required for good stress transfer,[19] and at least eight may be required to achieve the cohesive strength of the constituent polymers.[20−22] The number of entanglements can be estimated by comparing the thickness of the interphase with the radius of gyration $R_{g,e}$, corresponding to the entanglement molecular weight M_e. Taking an average value of 3 nm for $R_{g,e}$,[23] the number of entanglements across the interphase, estimated as $d_I/R_{g,e}$, is on the order of only 2−4 for polymer pairs with interphase thickness less than 11 nm. The number of entanglements across the interphase is estimated to be 9 and 11 for PC/PETG ($d_I = 27$ nm) and PMMA/SAN25 ($d_I = 33$ nm), respectively, which is more than the 8 entanglements required for achieving cohesive strength of the constituent polymers.

The interphase strength is measured by the standard T-peel method using films with relatively thick layers in order to confine fracture to a single interphase.[24,25] For PMMA/PS, PMMA/SAN30, and PC/SAN25 ($d_I < 11$ nm), examination of peeled specimens in the optical microscope confirms crack propagation along a single interphase. In the SEM, the peeled surface is featureless with no evidence of crazing on either side, which would be visible at the 10 μm size scale.[26] If a significant amount of one polymer is torn off during fracture, a surface technique such as photoacoustic FTIR is sensitive enough to detect the residue. However, virtually clean spectra are obtained for all the fracture surfaces. The combined observations from microscopy and FTIR indicate that the crack propagates through the interphase, and therefore the T-peel test measures the interfacial strength.

Fracture surfaces of PC/PMMA ($d_I = 10$ nm) show the characteristic rough texture of crazing, which indicates that fracture occurs with a significant amount of plastic deformation. The reported delamination toughness is about 950 J m^2,[27] much higher than the predicted interfacial strength of approximately 100 J m^2. This may be due to a small amount of transesterification at the PC/PMMA interphase with formation of covalent bonds between PC and PMMA. Fracture surfaces of PC/PETG ($d_I = 27$ nm) resemble those of PC/PMMA, indicating a large amount of plastic deformation. Peel arms of PMMA/SAN25 ($d_I = 33$ nm) broke during testing due to the combination of strong interfacial adhesion and the brittle nature of the materials.

The results for G_{IC} are summarized in Table 2, along with interphase strength for PETG/SAN polymer pairs determined previously.[4] The minor chain diffusion model predicts a relationship between interphase strength and interphase thickness of $G_{IC} \propto d_I^2$.[21] From the plot in Figure 5, it appears that the interfacial

strength conforms to the predicted squared dependence on d_I, especially for polymer pairs with relatively low G_{IC}.

Interphase Free Volume. The density of films with discrete layers ρ_d is compared with the density of films that are completely interphase material ρ_I in Table 2. The density of discrete-layer films conforms to the calculated value based on volume additivity of the constituents. The interphase density is consistently lower than ρ_d for PMMA/PS, PMMA/SAN25, and PMMA/SAN30. The largest decrease of 0.0026 g cm^{-3} occurs with PMMA/PS whereas the smallest decrease of 0.0017 g cm^{-3} occurs with PMMA/SAN25. Although the density change is relatively small, it is significant relative to the uncertainty in the density measurements of $\pm$0.0005 g cm^{-3}. Lower density of interphase materials suggests a gain in free volume compared to additive contributions of the constituents.

In contrast, interphase materials based on PC and PETG consistently exhibit ρ_I higher than ρ_d (Table 2). Density changes range from 0.0087 g cm^{-3} for PETG/SAN30 to 0.0009 g cm^{-3} for PETG/SAN25. For these polymer pairs, the free volume appears to decrease upon interphase mixing. The difference between ρ_d and ρ_I accounts for the difference between P_h and P_I. Thus, polymer pairs that exhibit ρ_I larger than ρ_d have P_I lower than P_h, and vice versa, polymer pairs that exhibit ρ_I lower than ρ_d have P_I higher than P_h (Table 2). The only exception is PC/SAN25. There may be more experimental uncertainty in permeability measurements of this highly permeable polymer pair.

Positron annihilation lifetime spectroscopy (PALS) is a powerful probe of free volume structure at the molecular scale.[28–31] Examination of the constituent polymers reveals that free volume hole size varies from 2.52 Å for PETG to 2.85 Å for PS (Table 1). Films with discrete layers possess a mean hole radius r_d that is close to the additive value based on the constituents (Table 2). Interphase materials of PMMA/SAN25 and PMMA/SAN30 exhibit hole size r_I that is larger than r_d. Although r_I cannot be determined directly for PMMA/PS, the value of r_I estimated from the film with the largest fraction of interphase is also larger than r_d. The opposite is true of interphase materials based on PC and PETG, which consistently exhibit r_I that is smaller than r_d.

If the density difference between discrete layers and interphase materials is solely due to differences in free volume hole size, the change in free volume from density should be related to the free volume hole size according to

$$\Delta\nu = \frac{4\pi N_0}{3}(r_d^3 - r_I^3) \tag{6}$$

where $\Delta\nu = \rho_d^{-1} - \rho_I^{-1}$ and N_0 is the number of free volume holes per gram of interphase, which is assumed to be constant. For all the systems except PMMA/PS, films with the thinnest layers are completely interphase. Therefore, the interphase density and free volume hole size are directly measured. In the case of the PMMA/PS a completely interphase film is not obtained. An additive model is used to estimate the interphase properties from measurements on a film with $d_0 = 7.3$ nm and interphase volume fraction of 84% with values reported in Table 2.

The change in volume upon formation of the interphase from density is compared with that from hole size

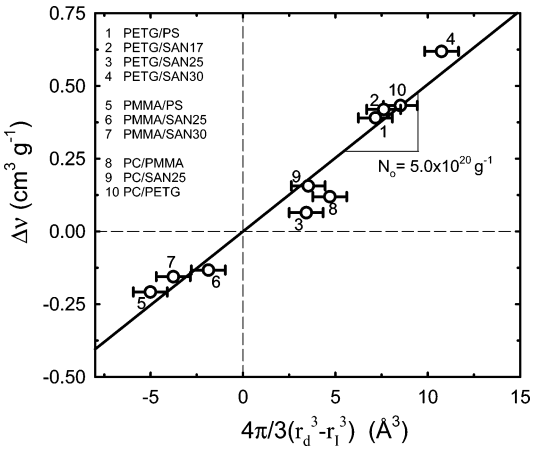

Figure 6. Deviation in interphase volume from the additive prediction based on constituent properties. The result from density is compared to the result from free volume hole size according to eq 6.

in Figure 6. The linear relationship confirms that the change in molecular scale free volume hole size is responsible for the observed change in density. Moreover, the plot provides a free volume hole density of 5.0×10^{20} g^{-1}, in good agreement with various PALS studies which consider either an average hole size,[31,32,33] or a distribution of hole sizes,[34] to arrive at a free volume hole density of about 4.0×10^{20} cm^{-3} at 23 °C for a wide range of polymers.

Interphase Glass Transition. The DMTA spectra of a PETG/SAN30 discrete layer film and a completely interphase film are compared in Figure 7a. The T_gs of PETG and SAN30 are clearly discerned in the spectrum of a film with discrete layers ($d_0 = 780$ nm). The lower intensity of the PETG tan δ peak is due to stress transfer from rubbery PETG layers to glassy SAN30 layers.[35] A single broad tan δ peak is observed at an intermediate temperature for PETG/SAN30 interphase material ($d_0 = 6$ nm). The peak temperature of the interphase material $T_{g,I}$ at 90 °C is somewhat lower the glass transition temperature of a homogeneous mixture $T_{g,h}$ of 102 °C, which is predicted by constituent additivity as

$$T_{g,h} = \omega_A T_{g,A} + \omega_B T_{g,B} \tag{7}$$

where ω_A and ω_B are the constituent weight fractions and $T_{g,A}$ and $T_{g,B}$ are the constituent T_gs. Similarly, a single broad tan δ peak at a temperature intermediate between the T_g peaks of the constituents is observed with all polymer pairs with either PC or PETG (Table 3). In all cases, the intermediate $T_{g,I}$ is lower than the prediction from eq 7.

Two T_gs can be distinguished in the DMTA spectrum of a PMMA/SAN30 film with discrete layers ($d_0 = 790$ nm), although the peaks are not well separated due to close proximity of the constituent T_gs (Figure 7b). The tan δ spectrum of PMMA/SAN30 interphase material ($d_0 = 6$ nm) exhibits a single broad, intense peak; however, in this case $T_{g,I}$ of 124 °C is higher than $T_{g,h}$ of 118 °C from eq 7. A single broad, intense $T_{g,I}$ peak at a temperature higher than $T_{g,h}$ is also characteristic of PMMA/SAN25 interphase materials (Table 3). Because of the small dimension of the PMMA/PS interphase ($d_I = 6.1$ nm), the film with the thinnest layers ($d_0 = 7.3$ nm) is only 84% interphase. However, the tan δ curve shows a single broad peak. It is assumed that the

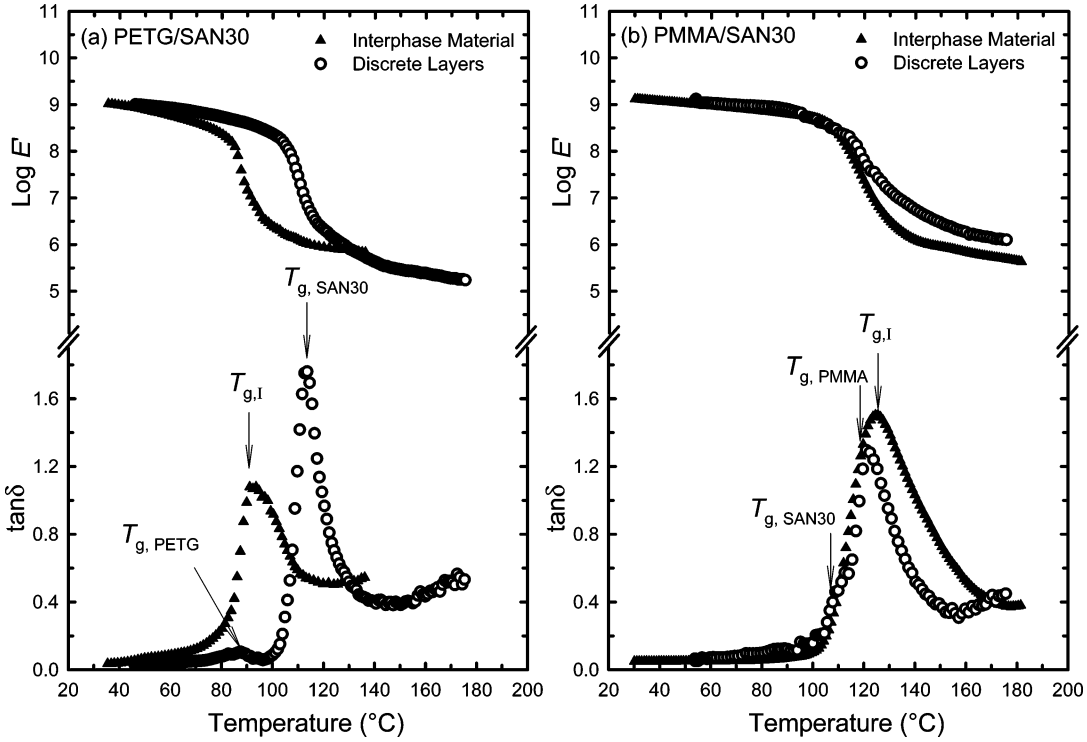

Figure 7. DMTA spectra of discrete layers and interphase materials: (a) PETG/SAN30 and (b) PMMA/SAN30.

Table 3. Physical Properties from Dynamical Mechanical Thermal Analysis

constituent polymers	T_g discrete layers (°C)	$T_{g,h}$[a] (°C)	$T_{g,I}$ interphase (°C)	log E_0 discrete layers (E_0 in Pa)	log E_0 interphase (E_0 in Pa)	$M_{e,d}$ (kg mol^{-1})	$M_{e,I}$ (kg mol^{-1})
PMMA/PS	118/109	114	125[b]	5.7	5.4[b]	5.7	11[b]
PMMA/SAN25	121/109	117	120	5.7	5.5	5.7	9.2
PMMA/SAN30	121/110	118	124	6.2	5.6	1.8	7.5
PC/PMMA	155/118	139	132	5.7	5.8	6.4	4.8
PC/PETG	158/90	122	120	5.7	6.2	6.1	1.8
PC/SAN25	159/118	136	133	5.5	5.6	11	8.2
PETG/PS	85/114	97	93[c]	5.2	5.6[c]	19	7.3[c]
PETG/SAN17	92/114	99	93	5.2	5.8	17	4.8
PETG/SAN25	84/115	101	98	5.4	5.5	12	9.1
PETG/SAN30	88/114	102	90	5.4	5.8	15	4.2

[a] From eq 7 using DMTA constituent T_g values in Table 1. [b] Film with 84% interphase. [c] Film with 76% interphase, ref 7.

contribution of the constituent layers is indiscernible in this case, and the peak temperature and plateau modulus of this film are taken as $T_{g,I}$ and E_0, respectively, of the PMMA/PS interphase.

If $T_{g,I}$ is lower than $T_{g,h}$, it means that the melt contracts further than expected along the equilibrium curve before it vitrifies. There is less free volume in the glass at ambient temperature as a consequence. The reverse is true if $T_{g,I}$ is higher than $T_{g,h}$. In this case, there is more free volume in the glass at ambient temperature. According to free volume concepts, the difference in specific free volume $\Delta\nu_f$ is related to the glass transition temperatures according to[36]

$$\Delta\nu_f = \Delta\alpha(T_{g,h} - T_{g,I}) \tag{8}$$

where $T_{g,h}$ is the additive result from eq 7, $T_{g,I}$ is the measured glass transition temperature of the interphase material, and $\Delta\alpha$ is the thermal expansivity difference between the rubbery and glassy states. Taking an average $\Delta\alpha$ from the literature as 3.0×10^{-4} cm^3 g^{-1} K^{-1},[15] the free volume difference from T_g according to eq 8 is compared with the specific volume difference from density $\Delta\nu$ in Figure 8. Reasonably good correspondence confirms the common source for the density deviation and the glass transition shift in free volume.

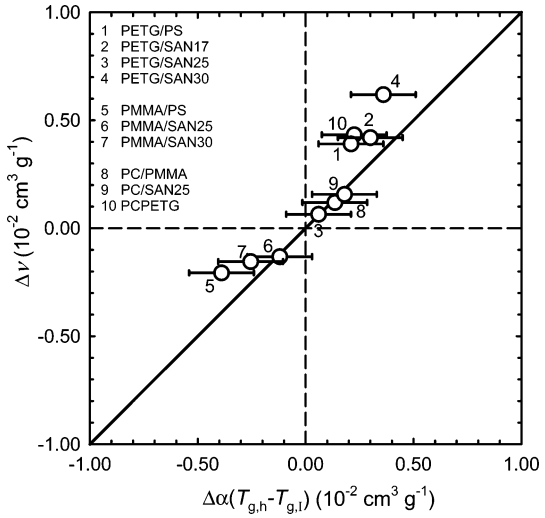

Figure 8. Comparison of the deviation in interphase specific volume from density and from glass transition temperature according to eq 8.

Interphase Chain Packing. It is also characteristic of interphase materials based on PETG and PC that they exhibit a weaker $T_{g,I}$ relaxation than the discrete

layer films, as illustrated for PETG/SAN30 in Figure 7a. The correspondingly smaller modulus drop for the interphase material is due to a higher plateau modulus E_0. Conversely, the stronger $T_{g,I}$ relaxation of PMMA/SAN30, PMMA/PS, and PMMA/SAN25 interphase materials compared to discrete layer films is accompanied by a larger modulus drop, which is due to a lower plateau modulus E_0, as shown in Figure 7b for PMMA/SAN30.

The rubbery plateau modulus is generally interpreted as the pseudoequilibrium modulus of the entanglement network and is directly related to the entanglement density according to[37]

$$M_e = \frac{3\rho RT}{E_0} \tag{9}$$

where ρ is the density, R is the gas constant, and T is the temperature. The rubbery plateau modulus from DMTA gives M_e values for the constituent polymers that are in reasonably good agreement with the literature values for PS, PC, and PMMA (Table 1). The entanglement molecular weights obtained from eq 9 for discrete layer films $M_{e,d}$ and for interphase materials $M_{e,I}$ are compared in Table 3. No direct correlation is observed between $M_{e,d}$ and M_e of the constituent polymers. Hence, $M_{e,d}$ is used only as a reference for $M_{e,I}$ of the corresponding interphase material. It is noted that if at least one of the paired polymers is PC or PETG, $M_{e,I}$ is lower than $M_{e,d}$. These are also the polymer pairs that experience a decrease in free volume upon interphase mixing, as determined by density, glass transition temperature, and free volume hole size. The opposite is the case for polymer pairs that combine PMMA with PS, SAN25, or SAN30, and $M_{e,I}$ is higher than $M_{e,d}$. These polymer pairs experience an increase in free volume upon interphase mixing, as determined by density, glass transition temperature, and free volume hole size.

It appears that interphase mixing alters the chain dimensions. For flexible polymers that take a random-coil sphere configuration, the chain dimension expressed as $\langle R^2\rangle_0/M$ determines the degree to which the coils interpenetrate and form entanglements. Here $\langle R^2\rangle_0$ is the unperturbed mean-square end-to-end distance, and M is the molecular weight. For PC and PET, the essentially temperature-independent value of $\langle R^2\rangle_0/M$ is reported to be about 1 Å^2 mol g^{-1}, and for PS and PMMA it is reportedly about 0.4 Å^2 mol g^{-1}.[38] The larger the dimension of the coil, the greater the volume it sweeps out. Therefore, the greater the number of other chains it encounters and with which it might entangle, hence the smaller M_e is.[38,39] According to this concept, polymers such as PC and PETG, with rigid in-chain phenyl groups separated by flexible linkages, tend to have a more expanded coil and lower M_e. Conversely, the flexible C−C backbone of PMMA, PS, and SAN leads to a smaller coil dimension and larger M_e.

It follows from comparison of $M_{e,I}$ and $M_{e,d}$ that if one or both of the constituent polymers tends to form an expanded coil in the melt, an even more expanded coil is obtained upon interphase mixing. Apparently, the more expanded coil can contract further along the equilibrium cooling curve before vitrification. This is indicated by lower free volume of the glassy interphase compared to the additive calculation. Conversely, interphase mixing of two compact polymer coils leads to an even more compact polymer coil in the melt. Higher free volume of the glassy interphase compared to the additive result signifies that the more compact coil cannot contract as far along the equilibrium cooling curve before vitrification.

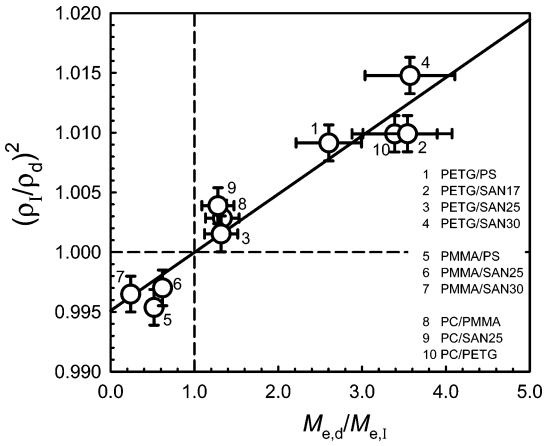

Figure 9. Relationship between relative entanglement molecular weight and relative density of interphase materials. The solid line represents the prediction given by eq 10.

The entanglement molecular weight of interphase material and discrete layer films should be related to the density according to[38,40,41]

$$\frac{M_{e,d}}{M_{e,I}} \propto \left(\frac{\rho_I}{\rho_d}\right)^2 \tag{10}$$

The results are plotted in Figure 9. Within the scatter, a reasonable linear relationship is obtained. The correlation supports speculation that interphase mixing of immiscible polymers results in alteration of the coil size, which in turn affects the vitrification temperature and free volume of the glass. Whether coil size increases or decreases apparently is not determined by the interaction parameter χ, at least not in a straightforward way, but does appear to depend on the coil characteristics of one or both of the constituents.

Conclusions

Forced assembly of immiscible polymers into layered nanostructures by layer-multiplying coextrusion makes it possible to probe the interphase with conventional tools of polymer analysis. Continuous layers in coextruded assemblies are revealed in AFM phase images. When individual layers are much thicker than the interphase dimension ($d_0 > 10d_I$), properties of the assembly follow additive predictions based on the constituent properties. As the layer thickness approaches the dimension of the polymer interphase ($d_I < d_0 \leq 10d_I$), the effects of interfacial molecular mixing are detected. Further reduction in layer thickness to the dimension of the interphase ($d_0 \leq d_I$) creates a new material that is entirely interphase. The interphase thickness, as determined from the layer thickness dependence of oxygen permeability, and interphase strength, as determined by the T-peel test, depend on interaction strength in accordance with model predictions based on the χ parameter.

Unexpectedly, volumetric properties of the interphase exhibit small but significant deviations from the additive predictions based on constituent properties. Correspondence between the variation in specific volume

from macroscopic density and the variation in free volume hole size from PALS suggests that interphase densification or dedensification occurs primarily by a change in free volume hole size rather than by a significant decrease in the number of free volume holes. The volume deviations account for a shift in glass transition temperature. However, the volumetric effects do not directly correlate with interaction strength as represented by the χ parameter.

A clue to the underlying cause of the volumetric deviations is found in the entanglement molecular weight, with reference to a model that identifies lower entanglement molecular weight with a more expanded polymer coil and the converse, a higher entanglement molecular weight with a more compact polymer coil. It is speculated that if at least one of the constituent polymers has an expanded coil, for example PC or PETG, interphase mixing leads to conformational changes that increase the size of the polymer coil. The opposite occurs if both of the constituent polymers have more compact coils, for example PMMA, PS, and SAN. In this case, conformational changes in the interphase produce an even more compact coil.

Acknowledgment. This research was generously supported by the NSF (Grant DMR-0349436, Polymers Program). Support from Modern Controls, Inc., for development of a facility for gas-transport studies at Case Western Reserve University is gratefully acknowledged.

References and Notes

(1) Paul, D. R., Bucknall, C. B., Eds.; *Polymer Blends;* Wiley: New York, 2000; Vols. 1 and 2.
(2) Helfand, E.; Sapse, A. M. *J. Chem. Phys.* **1975**, *62*, 1327−1331.
(3) Farinha, J. P. S.; Vorobyova, O.; Winnik, M. A. *Macromolecules* **2000**, *33*, 5863−5873.
(4) Jin, Y.; Rogunova, M.; Hiltner, A.; Baer, E.; Nowacki, R.; Galeski, A.; Piorkowska, E. *J. Polym. Sci., Part B: Polym. Phys.* **2004**, *42*, 3380−3396.
(5) Orench, I. P.; Ania, F.; Baer, E.; Hiltner, A.; Bernal, T.; Calleja, F. J. B. *Philos. Mag.* **2004**, *84*, 1841−1852.
(6) Liu, R. Y. F.; Jin, Y.; Hiltner, A.; Baer, E. *Macromol. Rapid Commun.* **2003**, *24*, 943−948.
(7) Liu, R. Y. F.; Bernal-Lara, T. E.; Hiltner, A.; Baer, E. *Macromolecules* **2004**, *37*, 6972−6979.
(8) Scheddel, R. T. *Anal. Chem.* **1958**, *30*, 1303−1303.
(9) Baer, E.; Kerns, J.; Hiltner, A. In *Structure Development During Polymer Processing*; Cunha, A. M., Fakirov, S., Eds.; Kluwer Academic Publishers: Dordrecht, 2000; pp 327−344.
(10) Mueller, C.; Kerns, J.; Ebeling, T.; Nazarenko, S.; Hiltner, A.; Baer, E. In *Polymer Process Engineering 97*; Coates, P. D., Ed.; Institute of Materials: London, 1997; pp 137−157.
(11) Higuchi, H.; Yu, Z.; Jamieson, A. M.; Simha, R.; McGervey, J. D. *J. Polym. Sci., Part B: Polym. Phys.* **1995**, *33*, 2295−2305.
(12) Helfand, E.; Tagami, Y. *J. Polym. Sci., Polym. Lett.* **1971**, *9*, 741−746.
(13) Helfand, E.; Tagami, Y. *J. Chem. Phys.* **1972**, *56*, 3592−3601.
(14) Helfand, E. *J. Chem. Phys.* **1975**, *63*, 2192−2198.
(15) Van Krevelen, D. W. *Properties of Polymers*, 3rd ed.; Elsevier: Amsterdam, 1997.
(16) Karam, H. J. In *Polymer Compatibility and Incompatibility: Principles and Practices*; Solc, K., Ed.; MMI Press: Chur, 1982; pp 93−106.
(17) Chen, H. Y.; Chum, S. P.; Hiltner, A.; Baer, E. *Macromolecules* **2001**, *34*, 4033−4042.
(18) Stephens, C. H.; Hiltner, A.; Baer, E. *Macromolecules* **2003**, *36*, 2733−2741.
(19) Creton, C.; Kramer, E. J.; Hadziioannou, G. *Macromolecules* **1991**, *24*, 1846−1853.
(20) Oslanec, R.; Brown, H. R. *Macromolecules* **2003**, *36*, 5839−5844.
(21) Wool, R. P. *Polymer Interfaces: Structure and Strength*; Hanser Publishers: Munich, 1995; Chapter 9, pp 336−376.
(22) Sperling, L. H. *Introduction to Physical Polymer Science*; John Wiley & Sons: New York, 2001; Chapter 11, pp 513−514.
(23) Sperling, L. H. *Introduction to Physical Polymer Science*; John Wiley & Sons: New York, 2001; Chapter 5, pp 165−200.
(24) Ebeling, T.; Hiltner, A.; Baer, E. *J. Appl. Polym. Sci.* **1998**, *68*, 793−805.
(25) Ebeling, T.; Hiltner, A.; Baer, E. *Polymer* **1999**, *40*, 1525−1536.
(26) Creton, C.; Kramer, E. J.; Hui, C. Y.; Brown, H. R. *Macromolecules* **1992**, *25*, 3075−3088.
(27) Kerns, J.; Hsieh, A.; Hiltner, A.; Baer, E. *J. Appl. Polym. Sci.* **2000**, *77*, 1545−1557.
(28) Ruan, M. Y.; Moaddel, H.; Jamieson, A. M.; Simha, R.; McGervey, J. D. *Macromolecules* **1992**, *25*, 2407−2411.
(29) McCullagh, C. M.; Yu, Z.; Jamieson, A. M.; Blackwell, J.; McGervey, J. D. *Macromolecules* **1995**, *28*, 6100−6107.
(30) Higuchi, H.; Jamieson, A. M.; Simha, R. *J. Polym. Sci., Part B: Polym. Phys.* **1996**, *34*, 1423−1426.
(31) Srithawatpong, R.; Peng, Z. L.; Olson, B. G.; Jamieson, A. M.; Simha, R.; McGervey, J. D.; Maier, T. R.; Halasa, A. F.; Ishida, H. *J. Polym. Sci., Part B: Polym. Phys.* **1999**, *37*, 2754−2770.
(32) Dlubek, G.; Bondarenko, V.; Pionteck, J.; Supej, M.; Wutzler, A.; Krause-Rehberg, R. *Polymer* **2003**, *44*, 1921−1926.
(33) Bamford, D.; Dlubek, G.; Reiche, A.; Alam, M. A.; Meyer, W.; Galvosas, P.; Rittig, F. *J. Chem. Phys.* **2001**, *115*, 7260−7270.
(34) Hong, X.; Jean, Y. C.; Yang, H. J.; Jordan, S. S.; Koros, W. J. *Macromolecules* **1996**, *29*, 7859−7864.
(35) Gregory, B.; Hiltner, A.; Baer, E. Im, J. *Polym. Eng. Sci.* **1987**, *27*, 568−572.
(36) Simha, R.; Boyer, R. F. *J. Chem. Phys.* **1962**, *37*, 1003−1007.
(37) Chen, H. Y.; Stepanov, E. V.; Chum, S. P.; Hiltner, A.; Baer, E. *Macromolecules* **2000**, *33*, 8870−8877.
(38) Fetters, L. J.; Lohse, D. J.; Richter, D.; Witten, T. A.; Zirkel, A. *Macromolecules* **1994**, *27*, 4639−4647.
(39) Witten, T. A.; Milner, S. T.; Wang, Z.-G. In *Multiphase Macromolecular Systems*; Culbertson, B. M., Ed.; Plenum: New York, 1989; pp 655−663.
(40) Ronca, G. *J. Chem. Phys.* **1983**, *79*, 1031−1043.
(41) Kavassalis, T. A.; Noolandi, J. *Macromolecules* **1988**, *21*, 2869−2879.

MA047292Z